

Topotactic Reduction of YBaCo₂O₅ and LaBaCo₂O₅: Square-Planar Co(I) in an Extended Oxide

James Seddon,[†] Emmanuelle Suard,[‡] and Michael A. Hayward^{*†}

*Department of Chemistry, Inorganic Chemistry Laboratory, University of Oxford,
South Parks Road, Oxford OX1 3QR, United Kingdom, and Institut Laue Langevin,
Avenue des Martyrs, B.P. 156, 38042 Grenoble Cedex 9, France*

Received November 30, 2009; E-mail: michael.hayward@chem.ox.ac.uk

Abstract: The low-temperature reduction of YBaCo₂O₅ and LaBaCo₂O₅ with NaH to form YBaCo₂O_{4.5} and YBaCo₂O_{4.25}, respectively, demonstrates that the structures of anion-deficient materials formed by such topotactic reductions can be directed by the ordering and identity of the A-site cations. YBaCo₂O_{4.5} adopts a structure consisting of a corner-shared network of square-based pyramidal CoO₅ and distorted tetrahedral CoO₄ units. The structure of LaBaCo₂O_{4.25} is more complex, consisting of an array of square-based pyramidal CoO₅, distorted tetrahedral CoO₄, and square planar CoO₄ units. Magnetic susceptibility and variable-temperature neutron diffraction data reveal that YBaCo₂O_{4.5} adopts a G-type antiferromagnetically ordered structure below $T_N \sim 280$ K. LaBaCo₂O_{4.25} also adopts antiferromagnetic order ($T_N \sim 325$ K) with ordered moments consistent with the presence of square-planar, low-spin, $s = 0$, Co(I) centers. A detailed analysis reveals that the different anion vacancy ordered structures adopted by the two REBaCo₂O_{5-x} phases are directed by the relative sizes and ordering of the La³⁺ and Y³⁺ cations. This suggests that ordered arrangements of A-cations can be used to direct the anion vacancy order in topotactically reduced phases, allowing the preparation of novel metal–oxygen networks containing unusual transition metal coordination environments.

Introduction

Complex transition metal oxides are of great importance from both an academic and a technological perspective due to the diverse range of physical properties they exhibit. Conventionally, the physical properties of complex oxides have been tuned by cation doping—the partial substitution of one metal for another. Recently, however, there has been a growing interest in manipulating and tuning the structures and physical behavior of complex oxides by modifying their anion lattices. One of the simplest ways of achieving this is by lowering the oxygen stoichiometry of materials, leading to the formation of “anion-deficient” phases. The lower oxygen stoichiometry in these phases necessarily leads to a reduction in the average oxidation states of transition metals present. In addition, anion-deficient phases contain vacant anion sites which lower metal coordination numbers and disrupt metal–anion–metal coupling networks. These influences, when combined, can radically change the magnetic coupling and electronic transport behavior of a material. In addition, the introduction of large numbers of vacant anion sites can enable fast ionic transport within anion-deficient phases.

The anion vacancies in anion-deficient phases can adopt a very large number of arrangements and varying degrees of order. If we restrict our thoughts to materials based on the ABO₃ cubic perovskite structure, it becomes clear that even in this small subset of anion-deficient phases, a very large number of different

vacancy ordering schemes are possible (see refs 1 and 2 for some examples). Given that the materials properties of anion-deficient phases depend strongly on the arrangement and ordering of the anion vacancies present, chemists must learn to control these features of anion-deficient materials if their full potential is to be exploited. Currently the synthesis of a particular anion vacancy arrangement “on demand” is highly challenging.

One strategy which can be utilized to direct the arrangement of anion vacancies within a material is to exploit the strong coupling between cation and anion lattices. If we take the isostructural materials La₂Co₂O₅,³ La₂Ni₂O₅,⁴ and La₂Cu₂O₅⁵ (Figure 1), we observe anion vacancy ordered structures which reflect the coordination preferences of the different transition metals present on the B-sites of the phases, as directed in some part by local crystal field considerations.

More subtle control can be achieved by utilizing combinations of B-cations. For example, A₂BB'O_{6-x} phases tend to adopt structures related to the mineral brownmillerite (Ca₂FeAlO₅) if the B' cation is a group 3 metal (Al, Ga, In) which adopts a stable tetrahedral coordination. Thus, through a synergic interaction between the anion and cation lattices, a structure with

- (1) Anderson, M. T.; Vaughey, J. T.; Poeppelmeier, K. R. *Chem. Mater.* **1993**, *5*, 151–165.
- (2) Antipov, E. V.; Abakumov, A. M.; Istomin, S. Y. *Inorg. Chem.* **2008**, *47*, 8543–8552.
- (3) Hansteen, O. H.; Fjellvag, H.; Hauback, B. C. *J. Solid State Chem.* **1998**, *141*, 411–417.
- (4) Alonso, J. A.; Martinez-Lope, M. J. *J. Chem. Soc., Dalton Trans.* **1995**, 2819–2824.
- (5) La Placa, S. J.; Bringley, J. F.; Scott, B. A.; Cox, D. E. *Acta Crystallogr. C* **1993**, *49*, 1415–1417.

[†] University of Oxford.

[‡] Institut Laue Langevin.

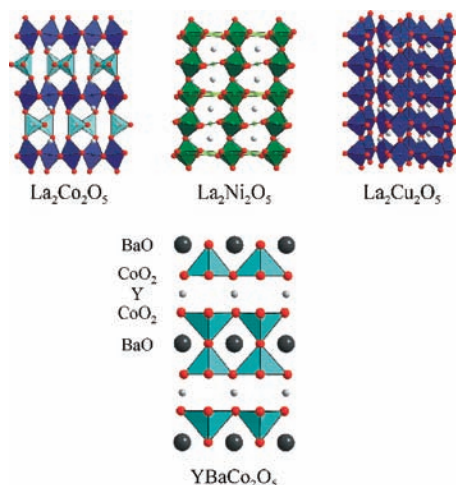


Figure 1. (Top) Structures of $\text{La}_2\text{Co}_2\text{O}_5$ (octahedral and tetrahedral cobalt), $\text{La}_2\text{Ni}_2\text{O}_5$ (octahedral and square-planar nickel), and $\text{La}_2\text{Cu}_2\text{O}_5$ (five-coordinate square-based pyramidal copper). (Bottom) Structure and A-cation ordering in YBaCo_2O_5 .

ordered anion vacancies and an ordered arrangement of B-cations is realized. A detailed discussion of the factors that drive the anion vacancy and cation ordering in brownmillerite-type phases is given in a recent review.²

Vacancies in the anion lattice can also direct ordering of the A-cations in perovskite phases. This order can be rationalized on the basis of “preferred” coordination numbers. A clear example of this behavior can be seen in the $\text{REBaM}_2\text{O}_{6-x}$ phases (RE = lanthanide, Y; M = Mn, Fe, Co).^{6–10} When these phases are prepared with close to complete oxygen stoichiometry ($x \approx 0$), cubic materials with disordered A-cation lattices are observed.^{11,12} However, when significantly anion-deficient materials are prepared ($x > 0.25$), an ordered structure is adopted with the A-cations ordered into layers and the anion vacancies arranged such that all the coordination sites of the large barium cations remain 12-coordinate, with the smaller RE cations located in sites of a lower coordination number (Figure 1). Indeed, the degree of oxygen nonstoichiometry can be used to reversibly control the degree of A-cation order, as observed recently in a related material, $\text{Ca}_2\text{Ba}_2\text{Nd}_2\text{Fe}_6\text{O}_{18-x}$.¹³

The phases discussed above are generally prepared at high temperature where both the anion and cation lattices are highly mobile and free to respond to the influences exerted upon them by any changes in anion stoichiometry. The resulting materials can be considered to have structures which have achieved an equilibrium between the directing influences of the anion and cation lattices. An alternative route to anion-deficient materials is low-temperature reduction. If anions are extracted from materials at a sufficiently low temperature, there is insufficient

thermal energy for the cation lattice to respond to changes in the anion lattice. As a result, these reductions tend to be topotactic—they conserve the structure and cation order or disorder of the host material. Phases formed by this method are often highly metastable with respect to decomposition to simpler binary oxide phases. In addition, they often exhibit unique metal–oxygen networks which have no high-temperature analogue.

The obvious strong coupling between the A-cation order and anion vacancy order in $\text{REBaCo}_2\text{O}_{6-x}$ phases^{6,14,15} suggests a similar influence should be exerted under low-temperature conditions and motivated us to investigate the influence of different ordered A-cations on the structures of materials prepared by low-temperature topotactic reduction. Recently we have employed binary metal hydrides to affect low-temperature topotactic reductions of complex transition metal oxides.^{16–18} Here we report the topotactic reduction of cation-ordered YBaCo_2O_5 and $\text{LaBaCo}_2\text{O}_5$ and discuss the role of the different A-cations in directing the anion vacancy order in the phases produced.

Experimental Section

Synthesis of YBaCo_2O_5 and $\text{LaBaCo}_2\text{O}_5$. Samples of YBaCo_2O_5 and $\text{LaBaCo}_2\text{O}_5$ were prepared by a citrate gel method. Suitable ratios of BaCO_3 (99.997%), cobalt metal (99.998%), and either Y_2O_3 or La_2O_3 (99.999% dried at 900 °C) were dissolved in a minimum quantity of a 1:1 mixture of 6 M nitric acid and distilled water. Three mole equivalents of citric acid and 5 mL of analar ethylene glycol were added, and the solution was heated with constant stirring. The gels thus formed were subsequently ground into a fine powder, placed in an alumina crucible, and heated at 1 °C min^{-1} to 900 °C in air to remove the remaining organic components from the samples.

The yttrium–barium samples were reground and pressed into 13 mm pellets with a force of 5 tonnes and heated under flowing oxygen for four periods of 24 h at 1000 °C with regrinding between heating periods to prepare $\text{YBaCo}_2\text{O}_{5.5}$. As a final step samples were heated for 10 h at 800 °C under flowing argon to ensure the formation of YBaCo_2O_5 . Samples were observed to be phase pure by laboratory X-ray powder diffraction, with lattice parameters ($a = 3.894(1)$ Å, $b = 3.888(1)$ Å, $c = 7.482(1)$ Å) in good agreement with published values.⁶

The lanthanum–barium calcined gels were treated in a manner similar to that described by Rautama et al.¹⁴ Samples were pressed into pellets and heated at 1100 °C for 48 h under an argon atmosphere which had been previously passed over titanium wire at 800 °C to remove any trace oxygen. Samples were then cooled at 1 °C min^{-1} to room temperature under argon to ensure cation-ordered samples were prepared. Samples were observed to be phase pure by laboratory X-ray powder diffraction, with lattice parameters $a = 3.9220(1)$ Å, $b = 3.9045(1)$ Å, $c = 8.0550(2)$ Å.

Reduction of YBaCo_2O_5 and $\text{LaBaCo}_2\text{O}_5$. The reduction of samples was performed using NaH (Aldrich >95%) as a solid-state reducing agent.¹⁶ Samples of YBaCo_2O_5 or $\text{LaBaCo}_2\text{O}_5$ were thoroughly ground in an argon-filled glovebox (O_2 and $\text{H}_2\text{O} < 1$

(6) Vogt, T.; Woodward, P. M.; Karen, P.; Hunter, B. A.; Henning, P.; Moodenbaugh, A. R. *Phys. Rev. Lett.* **2000**, *84*, 2969.

(7) Millange, F.; Suard, E.; Caignaert, V.; Raveau, B. *Mater. Res. Bull.* **1999**, *34*, 1.

(8) Caignaert, V.; Millange, F.; Domenges, B.; Raveau, B. *Chem. Mater.* **1999**, *11*, 930–938.

(9) Woodward, P. M.; Karen, P. *Inorg. Chem.* **2003**, *42*, 1121.

(10) Karen, P.; Suard, E.; Fauth, F.; Woodward, P. M. *Solid State Sci.* **2004**, *6*, 1195–1204.

(11) Fauth, F.; Suard, E.; Caignaert, V. *Phys. Rev. B* **2001**, *65*, 60401.

(12) Millange, F.; Caignaert, V.; Domenges, B.; Raveau, B.; Suard, E. *Chem. Mater.* **1998**, *10*, 1974.

(13) Tenailleau, C.; Allix, M.; Claridge, J. B.; Hervieu, M.; Thomas, M. F.; Hirst, J. P.; Rosseinsky, M. J. *J. Am. Chem. Soc.* **2008**, *130*, 7570–7583.

(14) Rautama, E.-L.; Caignaert, V.; Boullay, P.; Kundu, A. K.; Pralong, V.; Karppinen, M.; Ritter, C.; Raveau, B. *Chem. Mater.* **2009**, *21*, 102–109.

(15) Fauth, F.; Suard, E.; Caignaert, V.; Domenges, B.; Mirebeau, I.; Keller, L. *Eur. Phys. J. B* **2001**, *21*, 163–174.

(16) Hayward, M. A.; Green, M. A.; Rosseinsky, M. J.; Sloan, J. *J. Am. Chem. Soc.* **1999**, *121*, 8843–8854.

(17) Hayward, M. A.; Cussen, E. J.; Claridge, J. B.; Bieringer, M.; Rosseinsky, M. J.; Kiely, C. J.; Blundell, S. J.; Marshall, I. M.; Pratt, F. L. *Science* **2002**, *295*, 1882.

(18) Hadermann, J.; Abakumov, A.; Adkin, J. J.; Hayward, M. A. *J. Am. Chem. Soc.* **2009**, *131*, 10598–10604.

ppm) with a double stoichiometric quantity of NaH. The resulting mixtures were then sealed in evacuated Pyrex tubes and heated for three periods of 2 days at 210 °C with grinding between heating periods. Samples were then washed with 4×100 mL of methanol under nitrogen to remove sodium-containing phases (NaOH and NaH) before being dried under a vacuum.

Characterization. X-ray powder diffraction data were collected from samples contained within homemade air-sensitive sample holders utilizing a Panalytical X'pert diffractometer incorporating an X'celerator position-sensitive detector (monochromatic Cu $K_{\alpha 1}$ radiation). Neutron powder diffraction data were collected from samples contained in vanadium cans which had been sealed under argon with an indium washer. Initially data were collected using the POLARIS instrument at the ISIS neutron source (Rutherford Appleton Laboratory, UK) at 2 and 298 K. Additional data sets were collected using the D2b diffractometer at the ILL neutron source (Grenoble, France) ($\lambda = 1.59$ Å) from $\text{YBaCo}_2\text{O}_{5-x}$ at temperatures between 5 and 300 K using a closed-cycle cryostat and from $\text{LaBaCo}_2\text{O}_{5-x}$ between 5 and 350 K using a cryofurnace. Rietveld structural refinements were performed against X-ray or neutron powder diffraction data utilizing the GSAS suite of programs.¹⁹ Electron diffraction data were collected from finely ground samples supported on lacy carbon grids (deposited from suspension in methanol) using a JEOL 2000FX microscope operating at 200 kV. Thermogravimetric reduction measurements were performed under a flowing atmosphere of 5% H_2 in N_2 on powder samples using a Netzsch STA 409PC balance. Magnetization measurements were collected using a Quantum Design MPMS SQUID magnetometer. Magnetization data indicated that all the reduced samples contained small quantities of ferromagnetic elemental cobalt, which masked the magnetic behavior of the bulk phases. The paramagnetic susceptibility of samples was therefore measured using a “ferromagnetic subtraction” technique described previously²⁰ and described fully in the Supporting Information.

Results

X-ray powder diffraction data collected from $\text{YBaCo}_2\text{O}_{5-x}$ and $\text{LaBaCo}_2\text{O}_{5-x}$ can be indexed with simple orthorhombic unit cells ($\text{YBaCo}_2\text{O}_{5-x}$: $a \approx 4.12$ Å, $b \approx 3.67$ Å, $c \approx 7.58$ Å; $\text{LaBaCo}_2\text{O}_{5-x}$: $a \approx 4.19$ Å, $b \approx 3.86$ Å, $c \approx 7.66$ Å). These data are consistent with simple topotactic reductions of the $\text{REBaCo}_2\text{O}_5$ phases. Thermogravimetric reductions with dilute hydrogen, to form BaO, RE_2O_3 , and elemental cobalt, yielded compositions of $\text{YBaCo}_2\text{O}_{4.505(5)}$ and $\text{LaBaCo}_2\text{O}_{4.251(5)}$. The thermogravimetric data (Supporting Information) exhibit a number of plateaus at intermediate mass, suggesting intermediate phases have been formed. However, X-ray diffraction data reveal the mixtures present at these plateaus do not contain any quaternary phases and occur due to complex decomposition routes involving both reduction and disproportionation.

Structural Characterization of $\text{YBaCo}_2\text{O}_{4.5}$. Due to the low sensitivity of X-ray diffraction data to the location of light atoms (oxygen) in the presence of heavy atoms (barium), neutron and electron diffraction data were collected from $\text{YBaCo}_2\text{O}_{4.5}$ to unambiguously determine the crystal structure of the phase. Both room-temperature electron and neutron diffraction data collected from $\text{YBaCo}_2\text{O}_{4.5}$ exhibited additional diffraction features consistent with a monoclinic expansion of the crystallographic unit cell relative to the cell determined from the X-ray powder diffraction data ($a = 8.2668(4)$ Å, $b = 3.6818(1)$ Å, $c = 8.6474(5)$ Å, $\beta = 118.51(1)^\circ$). Figure 2 shows representative

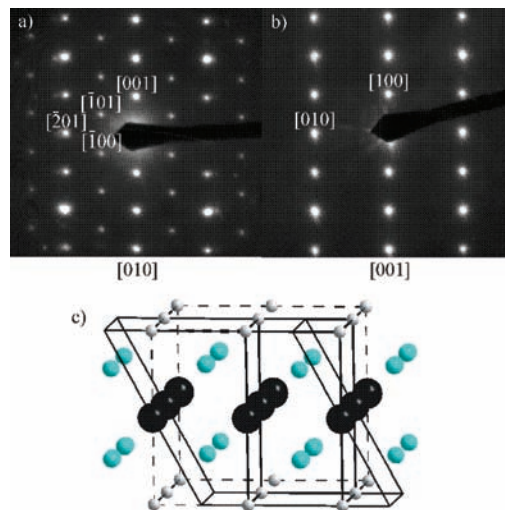


Figure 2. Electron diffraction data from the (a) [010] and (b) [001] zone axes of $\text{YBaCo}_2\text{O}_{4.5}$. (c) Geometric relations between the unit cells of $\text{YBaCo}_2\text{O}_{4.5}$ determined by X-ray diffraction (small orthorhombic) and neutron and electron diffraction (monoclinic). The larger orthorhombic magnetic unit cell is indicated with a dashed line.

electron diffraction data and the geometric relationship between the orthorhombic and monoclinic cells of $\text{YBaCo}_2\text{O}_{4.5}$.

A model based on the A-cation ordered structure of YBaCo_2O_5 was constructed within this monoclinic cell. This model was refined against room-temperature neutron diffraction data collected using the POLARIS diffractometer. Initially the positional and displacement parameters of all the atoms within the model were refined. Subsequently the anion occupancy factors were refined to locate the anion vacancies within the structure. This led to the rapid decline of the occupation factor of the anion at ($\sim 0.5, 0, z$) to almost exactly one-half, consistent with an overall sample stoichiometry of $\text{YBaCo}_2\text{O}_{4.5}$. Examination of the displacement ellipsoid of the cobalt center directly bonded to the partially vacant anion site (Co(2)) revealed it was anomalously large, suggesting static disorder. This site was therefore split either side of the $y = 1/2$ mirror plane and set to half occupancy. This led to a significant improvement to the fit (χ^2 dropped from 2.3 to 1.9). Close inspection of the neutron diffraction data revealed a number of weak reflections not indexed by the model. These could be accounted for by an orthorhombic phase ($a = 3.9297(3)$ Å, $b = 3.8658(3)$ Å, $c = 7.603(1)$ Å) which was taken to be a small amount of incompletely reduced material. A model corresponding to this phase was added to the refinement model to account for these diffraction features. However, due to the low concentration of this impurity phase in the sample, none of its structural parameters, with the exception of the lattice parameters, could be refined. The two-phase refinement converged readily, yielding a goodness of fit $\chi^2 = 1.718$. Details of the refined phases are given in Table 1, with observed, calculated, and difference plots from the refinement given in the Supporting Information. Representations of the refined structure of $\text{YBaCo}_2\text{O}_{4.5}$ are shown in Figure 3.

Magnetic Characterization of $\text{YBaCo}_2\text{O}_{4.5}$. Magnetic susceptibility data collected from $\text{YBaCo}_2\text{O}_{4.5}$ via the “ferromagnetic subtraction” method described above are shown in Figure 4. It can be seen that there is a large drop in the magnetic susceptibility of $\text{YBaCo}_2\text{O}_{4.5}$ at $T \sim 280$ K and a further local maximum at $T \sim 25$ K. Examination of neutron diffraction data collected from $\text{YBaCo}_2\text{O}_{4.5}$ at 5 K (D2b) reveals a number of

(19) Larson, A. C.; Von Dreele, R. B. *General Structure Analysis System*; Los Alamos National Laboratory Report LAUR 86-748, 2000.

(20) Hayward, M. A.; Rosseinsky, M. J. *Chem. Mater.* **2000**, *12*, 2182–2195.

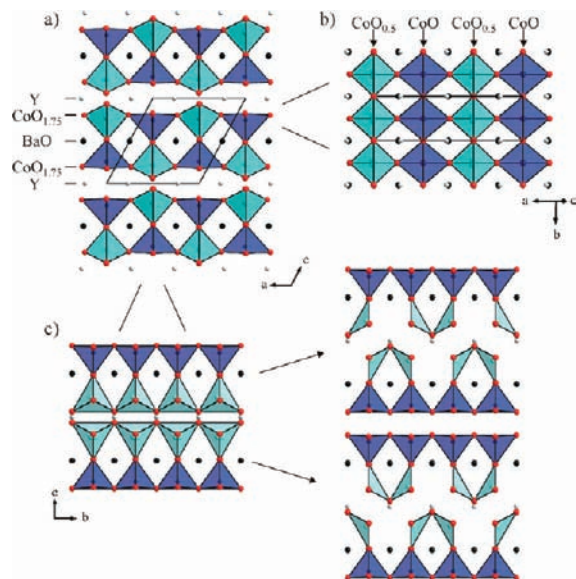
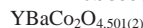


Figure 3. Refined structure of YBaCo₂O_{4.5} (a) shown in projection viewed along the *y*-axis. (b) A view of the CoO_{1.75} anion-deficient plane. (c) A projection viewed along the *x*-axis with expansions showing the two possible ordered anion vacancy arrangements.

Table 1. Structural Parameters from the Two-Phase Refinement of YBaCo₂O_{4.501(2)} at 298 K

atom	<i>x</i>	<i>y</i>	<i>z</i>	occupancy	<i>U</i> _{iso} (Å ³)
Ba(1)	0	0	1/2	1	0.0088(2)
Ba(2)	1/2	0	1/2	1	0.0088(2)
Y(1)	0.2308(4)	0	0.9999(8)	1	0.0056(1)
Co(1)	0.131(1)	1/2	0.2568(2)	1	0.0050(4)
Co(2)	0.610(2)	0.4456(8)	0.2264(3)	0.5	0.0080(7)
O(1)	0.2544(7)	1/2	0.5146(1)	1	0.0091(2)
O(2)	0.3606(6)	1/2	0.1967(6)	1	0.0083(1)
O(3)	0.8306(6)	1/2	0.1924(6)	1	0.0083(1)
O(4)	0.0856(7)	0	0.1778(1)	1	0.0085(2)
O(5)	0.465(1)	0	0.9355(2)	0.501(2)	0.0100(5)



space group *P2/m*, *a* = 8.2668(4) Å, *b* = 3.6818(1) Å, *c* = 8.6474(5) Å
 $\beta = 118.51(1)^\circ$, cell volume = 231.28(3) Å³

mole fraction 95.1(2)%

Ba(1)	0	0	0	1	0.031(1)
Y(1)	0	0	1/2	1	0.031(1)
Co(1)	1/2	1/2	0.259	1	0.031(1)
O(1)	1/2	1/2	0	1	0.031(1)
O(2)	0	1/2	0.312	1	0.031(1)
O(3)	1/2	0	0.312	1	0.031(1)



space group *Pmmm*, *a* = 3.9297(3) Å, *b* = 3.8658(3) Å, *c* = 7.603(1) Å
 cell volume = 115.52(2) Å³

mole fraction 4.9(2)%

$\chi^2 = 1.718$, *wR*_p = 2.01%, *R*_p = 3.29%

additional low-angle diffraction peaks with respect to an analogous data set collected at 298 K (Figure 5), which can be indexed with an orthorhombic cell related to the monoclinic crystallographic cell as shown in Figure 2. The intensities of the observed magnetic diffraction peaks are accounted for well by a simple G-type antiferromagnetic model with the moments directed along the *b*-axis (Figure 6a). Refinement of this model against neutron diffraction data collected at 5 K yielded an ordered moment of 3.29(3) μ_B per cobalt center, consistent with an array of Co(II) centers with unquenched orbital moments. Refinement of analogous magnetic models against data sets collected at 200 and 250 K yielded ordered moments of 2.82(3)

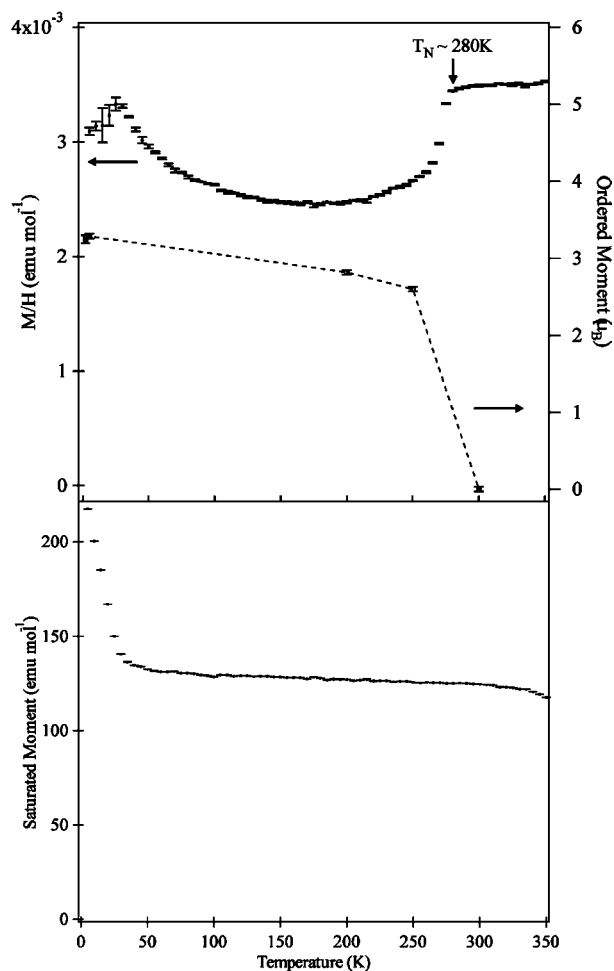


Figure 4. (Top) Plot of the magnetic susceptibility of YBaCo₂O_{4.5} measured by the “ferromagnetic subtraction” method (left) and the ordered moment per cobalt (right) as a function of temperature. (Bottom) Plot of the saturated ferromagnetic moment as a function of temperature.

and 2.60(3) μ_B , respectively. These values are consistent with the magnetic susceptibility anomaly observed at 280 K being associated with the onset of antiferromagnetic order (*T*_N), as shown in Figure 4. There appears to be no significant change in the magnitude of the local ordered moment associated with the susceptibility anomaly observed at *T* ~ 25 K (Figure 4). However, the saturated magnetic moment (measured as the zero-field intercept of the linear fit to the magnetization-field isotherm at a given temperature; Figure 4) shows a significant rise around this temperature, suggesting the local susceptibility maximum is associated with a spin canting transition. However, it was not possible to model this spin canting in the ordered magnetic models. Full details of the structural and magnetic refinements performed against data collected at 5, 200, and 250 K are given in the Supporting Information.

Characterization of LaBaCo₂O_{4.25}. The structure of LaBaCo₂O_{4.25} is more complex than that of YBaCo₂O_{4.5}. Electron diffraction data collected from LaBaCo₂O_{4.25} (Figure 7) are consistent with an orthorhombic unit cell (*a* = 16.922(5) Å, *b* = 7.785(2) Å, *c* = 15.463(5) Å) which corresponds to a 4 × 2 × 2 expansion of the cell determined by X-ray powder diffraction. Neutron diffraction data collected from LaBaCo₂O_{4.25} are also consistent with this expanded cell, most obviously by the presence of a diffraction peak at *d* = 7.7 Å, which corresponds to the [101] reflection of the expanded cell (Figure

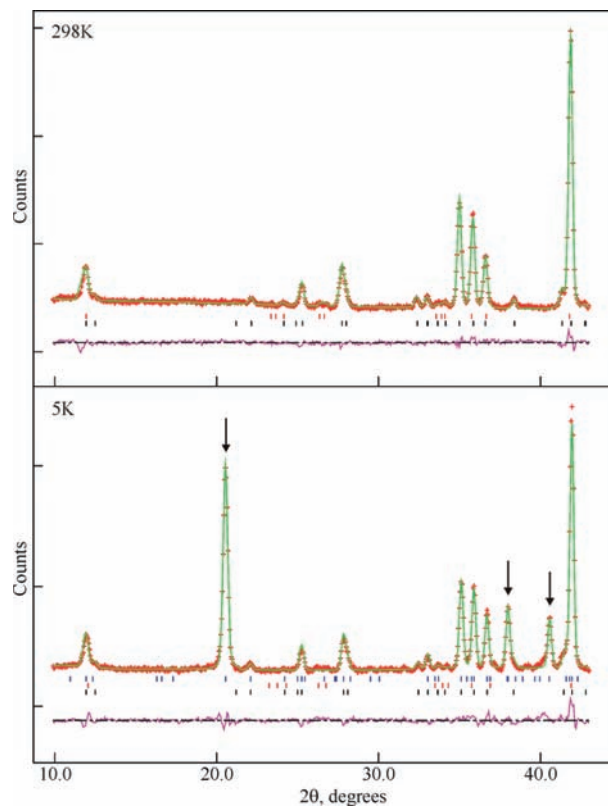


Figure 5. Observed, calculated and difference plots from the structural and magnetic refinements of $\text{YBaCo}_2\text{O}_{4.5}$ against neutron powder diffraction data collected at 298 (top) and 5 K (bottom). Arrows mark strong magnetic reflections.

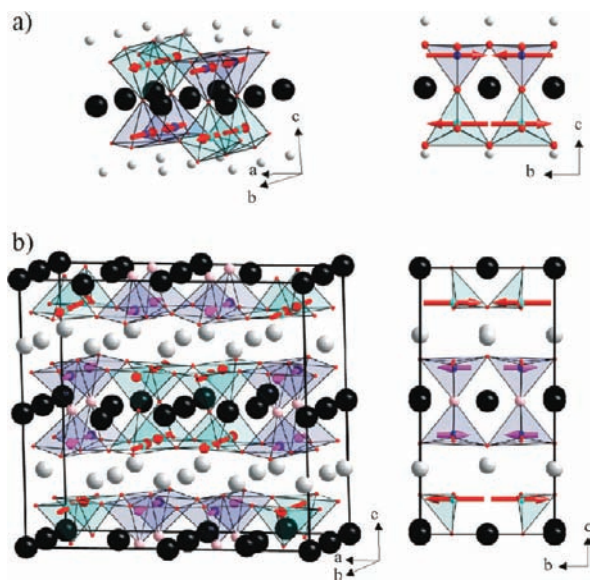


Figure 6. (a) Refined magnetic structure of $\text{YBaCo}_2\text{O}_{4.5}$ showing a simple G-type antiferromagnetic order. Ordered moment at 5 K is $3.29(3) \mu_B$. (b) Refined magnetic structure of $\text{LaBaCo}_2\text{O}_{4.25}$ showing G-type antiferromagnetic order. Ordered moment at 5 K of tetrahedral sites (red arrows) is $3.31(2) \mu_B$, and of planar/pyramidal sites (pink arrows) is $1.61(2) \mu_B$.

8). The reflection conditions derived from the electron diffraction data are as follow: hkl , no conditions; $0kl$, $l = 2n$; $h0l$, no conditions; $hk0$, $h = 2n$; $h00$, $h = 2n$; $0k0$, no conditions; $00l$, $l = 2n$. These reflection conditions correspond to the extinction symbol Pc_a , corresponding to the possible space groups $Pcma$ and $Pc2a$.

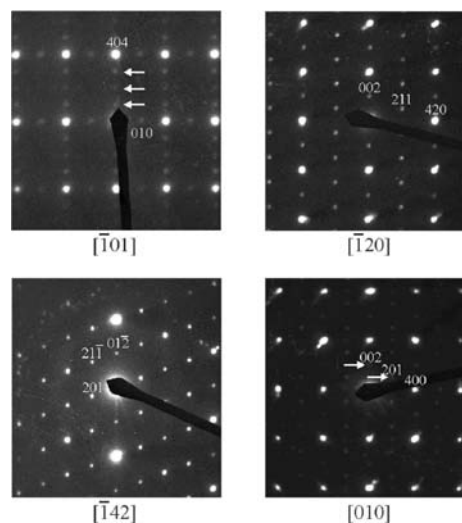


Figure 7. Electron diffraction data collected from $\text{LaBaCo}_2\text{O}_{4.25}$ consistent with an orthorhombic unit cell: $a = 16.92 \text{ \AA}$, $b = 7.78 \text{ \AA}$, $c = 15.46 \text{ \AA}$.

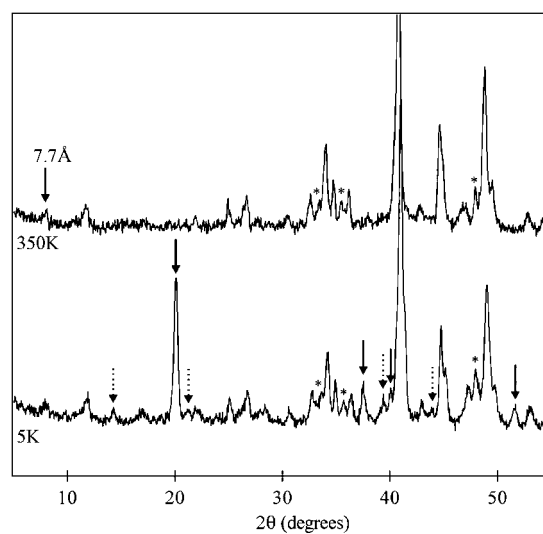


Figure 8. Neutron powder diffraction data collected from $\text{LaBaCo}_2\text{O}_{4.25}$ at 5 and 350 K. Solid arrows mark diffraction peaks due to simple G-type antiferromagnetic order. Dashed arrows show additional weak diffraction peaks indicating larger magnetic unit cell. Stars correspond to peaks from an impurity phase present at both temperatures.

Examination of magnetic susceptibility data collected from $\text{LaBaCo}_2\text{O}_{4.25}$ using the “ferromagnetic subtraction” technique (Figure 9) reveals a local maximum at $T \sim 325 \text{ K}$. Comparison of neutron diffraction data sets collected at 350, 298, and 5 K (Figure 8) reveals a series of additional diffraction peaks at large d -spacing in the data sets collected below 325 K, consistent with the onset of magnetic order at this temperature.

A crystallographic model based on the structure of $\text{LaBaCo}_2\text{O}_5$ (isostructural with YBaCo_2O_5) was constructed in the space group $Pcma$ within the expanded orthorhombic cell determined for $\text{LaBaCo}_2\text{O}_{4.25}$. A simple G-type antiferromagnetic model based on the magnetic model refined for $\text{YBaCo}_2\text{O}_{4.5}$ was initially used to account for the observed magnetic diffraction features in the room-temperature neutron diffraction data, as will be discussed fully later.

Examination of Fourier difference plots and the subsequent refinement of the occupation factors of equatorial anion sites led to the refinement of an ordered array of fully occupied and empty anion sites in the equatorial CoO_{2-x} plane. The refined

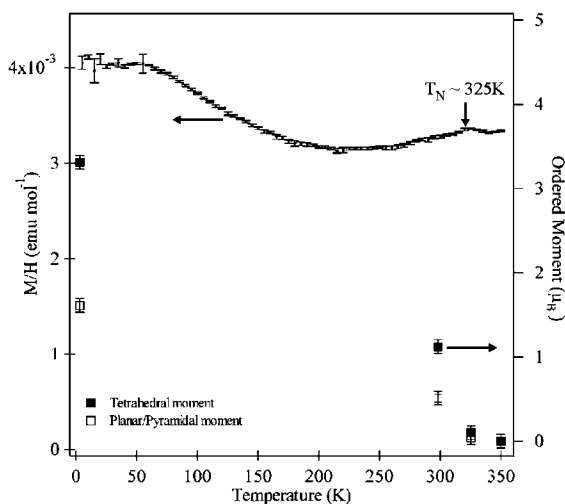


Figure 9. Plot of the magnetic susceptibility of $\text{LaBaCo}_2\text{O}_{4.25}$ measured by the “ferromagnetic subtraction” method and the ordered moment per cobalt as a function of temperature.

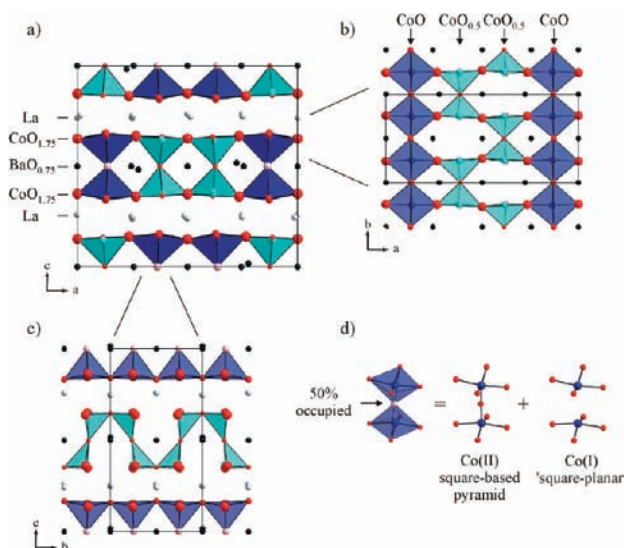


Figure 10. Refined structure of $\text{LaBaCo}_2\text{O}_{4.25}$: (a) projection viewed along the y -axis; (b) a view of the $\text{CoO}_{1.75}$ anion-deficient plane; (c) projection viewed along the x -axis. (d) Partial occupancy of the axial anion site leads to the superposition of square-planar and square-based pyramidal cobalt coordination sites.

structure at this stage consisted of an ordered array of four-coordinate “tetrahedral” and five-coordinate “square-based pyramidal” cobalt centers and an overall sample stoichiometry of $\text{LaBaCo}_2\text{O}_{4.5}$. Further Fourier difference plots indicated that the apical anion sites (those in the BaO layers) were not fully occupied, and refinement of the occupation factors of these sites resulted in the “removal” of half the anions from the site which connected the previously five-coordinate cobalt centers ($\text{O}(12)$), lowering the overall sample stoichiometry to $\text{LaBaCo}_2\text{O}_{4.25}$, consistent with the thermogravimetric data. The structural model formed has cobalt in three different coordination environments: four-coordinate “tetrahedral” (50%); four-coordinate “square-planar” (25%), and five-coordinate “square-based pyramidal” (25%), with the location of the square-based pyramidal and square-planar environments being disordered (Figure 10). An analogous structural model constructed in the space group $Pc2a$ is compatible with ordering of the square-based pyramidal and square-planar coordination sites within the structure. However,

refinement of such a model against the neutron diffraction data also resulted in the refinement of a disordered structure. Given that the model in the space group $Pc2a$ has far fewer variables than that in $Pc2a$, the former model was retained. Finally, the atomic positional and displacement parameters of all atoms were refined. Initially hard constraints were applied to maintain the local symmetry of the cobalt coordination polyhedra in order to improve refinement stability. As the refinement progressed these constraints were gradually removed until ultimately all the atomic positions were refining freely.

In order to complete the refinement of $\text{LaBaCo}_2\text{O}_{4.25}$, the magnetic structure was examined in detail. Comparison of neutron diffraction data collected from $\text{LaBaCo}_2\text{O}_{4.25}$ at 350 and 5 K (Figure 8) reveals a series of strong additional diffraction features in the low-temperature data set, the intensity of which can be modeled well by a simple G-type antiferromagnetic structure analogous to that refined for $\text{YBaCo}_2\text{O}_{4.25}$. More detailed inspection of the neutron data reveals a further set of much weaker diffraction reflections (Figure 8), which can be indexed by the crystallographic unit cell. Using representational analysis to assess the magnetic models consistent with the crystal symmetry yielded an unworkably large number of possible magnetic structures. To simplify the problem, only model structures that were a small perturbation of a simple G-type antiferromagnetic model were considered. This allowed the refinement of a magnetic model based on a simple G-type antiferromagnetically ordered arrangement, but in which the four/five-coordinate cobalt centers had an ordered moment that was different from that of the four-coordinate tetrahedral centers (Figure 6b). Refinement of this magnetic model against the 5 K neutron diffraction data collected from $\text{LaBaCo}_2\text{O}_{4.25}$ yielded ordered moments of 1.61(2) and 3.31(2) μ_B for the four/five-coordinate and tetrahedral sites, respectively. This more complex magnetic description was added to the model refined against the room-temperature neutron diffraction data, which converged rapidly. Full details of the refined room-temperature crystal structure of $\text{LaBaCo}_2\text{O}_{4.25}$ are given in Table 2, with a complete description of the magnetic structure (5 K) given in the Supporting Information. Representations of the refined structure of $\text{LaBaCo}_2\text{O}_{4.25}$ are shown in Figure 10. A plot of the ordered magnetic moments as a function of temperature for $\text{LaBaCo}_2\text{O}_{4.25}$ is shown in Figure 9. Observed calculated and difference plots for the refinements at all temperatures are given in the Supporting Information.

Discussion

The anion-deficient structures of $\text{YBaCo}_2\text{O}_{4.5}$ and $\text{LaBaCo}_2\text{O}_{4.25}$ share a number of common features. If we consider the structures of these cation ordered phases as a series of stacked layers, we can express the structures of the $\text{REBaCo}_2\text{O}_5$ starting materials as the stacking sequence RE- CoO_2 -BaO- CoO_2 -RE- (Figure 1). Thus we can describe the structure of $\text{YBaCo}_2\text{O}_{4.5}$ as Y- $\text{CoO}_{1.75}$ -BaO- $\text{CoO}_{1.75}$ -Y- (Figure 3a) and that of $\text{LaBaCo}_2\text{O}_{4.25}$ as La- $\text{CoO}_{1.75}$ -BaO_{0.75}- $\text{CoO}_{1.75}$ -La- (Figure 10a). Examination of the $\text{CoO}_{1.75}$ layers common to both reduced phases reveals that the anion vacancies within these layers are present in the O-Co-O-Co chains which run parallel to the y -axis within each layer, resulting in rows of composition CoO and $\text{CoO}_{0.5}$ (Figures 3b and 10b). In the structure of $\text{YBaCo}_2\text{O}_{4.5}$ these rows are arranged in an alternating ABAB pattern along the x -axis. In contrast, an AABBAABB pattern is adopted by $\text{LaBaCo}_2\text{O}_{4.25}$ (Figures 3b and 10b). The relative arrangement of CoO and $\text{CoO}_{0.5}$ rows along the

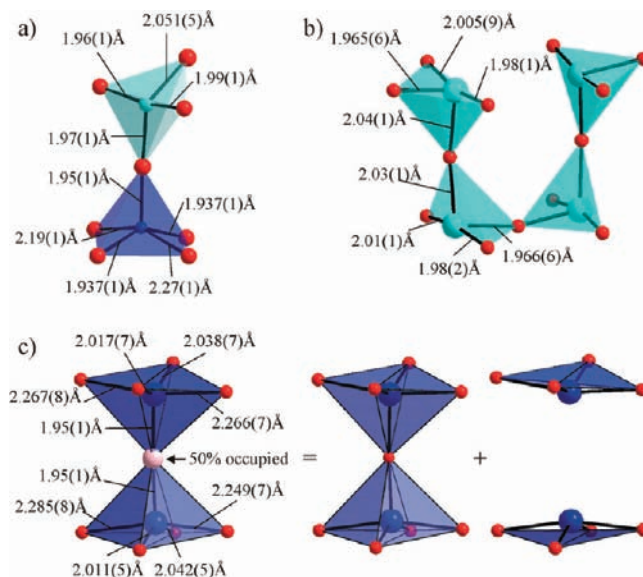
Table 2. Structural Parameters from the Refinement of LaBaCo₂O_{4.251(3)} at 298 K

atom	x	y	z	fraction	U _{iso} (Å ³)
Ba(1)	0	0	0	1	0.0074(1)
Ba(2)	0	0.5	0	1	0.0074(1)
Ba(3)	0.2232(5)	0	0.0167(7)	1	0.0074(1)
Ba(4)	0.2554(6)	0.5	0.000(1)	1	0.0074(1)
Ba(5)	0.5	0	0	1	0.0074(1)
Ba(6)	0.5	0.5	0	1	0.0074(1)
La(1)	0.0135(4)	0	0.2463(5)	1	0.0078(1)
La(2)	0.0009(5)	0.5	0.2591(5)	1	0.0078(1)
La(3)	0.2513(6)	0	0.2484(8)	1	0.0078(1)
La(4)	0.2497(5)	0.5	0.2590(7)	1	0.0078(1)
Co(1)	0.1170(5)	0.2503(8)	0.1314(7)	1	0.0125(3)
Co(2)	0.8834(6)	0.2496(8)	0.1314(7)	1	0.0125(3)
Co(3)	0.3675(4)	0.2505(5)	0.1268(5)	1	0.0125(3)
Co(4)	0.6335(4)	0.2512(8)	0.1268(5)	1	0.0125(3)
O(1)	0.000(1)	0.2698(8)	0.1387(4)	1	0.0101(6)
O(2)	0.2342(2)	0.2480(8)	0.1504(2)	1	0.0101(6)
O(3)	0.500(1)	0.2425(8)	0.1375(3)	1	0.0101(6)
O(4)	0.7657(2)	0.2480(9)	0.1504(2)	1	0.0101(6)
O(5)	0.1146(3)	0	0.1476(3)	1	0.0080(3)
O(6)	0.8853(3)	0.5	0.1476(3)	1	0.0080(3)
O(7)	0.3693(5)	0	0.1586(4)	1	0.0084(2)
O(8)	0.3718(5)	0.5	0.1673(4)	1	0.0084(2)
O(9)	0.6306(5)	0	0.1586(4)	1	0.0084(2)
O(10)	0.6281(5)	0.5	0.1673(4)	1	0.0084(2)
O(11)	0.1256(6)	0.2362(8)	0.9999(8)	1	0.0078(3)
O(12)	0.3636(2)	0.2550(9)	0.0002(9)	0.503(5)	0.0078(3)

LaBaCo₂O_{4.251(3)}
 space group *Pcma*, *a* = 16.922(5) Å, *b* = 7.785(2) Å, *c* = 15.463(5) Å
 ordered moment = 1.12(3) μ_B (tetrahedral), 0.51(3) μ_B
 four-/five-coordinate
 χ² = 2.14, wRp = 2.92%, Rp = 4.91%

structural stacking direction is also different for the two reduced phases. In the structure of YBaCo₂O_{4.5}, like rows are separated by yttrium layers and unlike rows by barium–oxygen layers (Figure 3a), giving a, A-Y-A-BaO-B-Y-B-BaO-A-Y-A sequence. The arrangement in LaBaCo₂O_{4.25} is reversed: like rows are separated by barium–oxygen layers and unlike rows by lanthanum layers, giving A-La-B-BaO_{0.75}-B-La-A-BaO_{0.75}-A-La-B sequence (Figure 10a).

Cobalt Coordination Environments in YBaCo₂O_{4.5}. The differing vacancy order patterns present in YBaCo₂O_{4.5} and LaBaCo₂O_{4.25} lead to significantly different cation coordinations and cation–anion–cation networks in the two phases. Considering YBaCo₂O_{4.5} first, the introduction of anion vacancies into the CoO_{1.75} layers leads to the conversion of half the square-based pyramidal cobalt centers present in YBaCo₂O₅ into four-coordinate sites. It can be seen from the refined structure that the locations of the anion vacancies within the CoO_{0.5} rows present in the CoO_{1.75} layers are disordered (Figure 3c). However, this disordered arrangement of vacancies can be seen as the superposition of two equivalent ordered anion vacancy arrangements in which alternate anion sites along the CoO_{0.5} rows are vacant, resulting in the formation of pairs of corner-linked, heavily distorted CoO₄ tetrahedra. Further inspection reveals that the oxide ions that link neighboring CoO₄ units within the CoO_{0.5} rows (O(5)) have been pushed into the yttrium layer to help satisfy the coordination requirements of yttrium and cobalt, as discussed more fully below. This has the effect of organizing the anion vacancies in pairs of neighboring CoO₄ chains, which lie on either side of an yttrium layer, to be “out of phase” with each other such that each yttrium center is seven-coordinate, as shown in Figure 3. The lack of evidence for long-range order in the arrangement of anion vacancies of YBaCo₂O_{4.5} suggests that, while each pair of CoO₄ chains may

**Figure 11.** Cobalt coordination polyhedra in (a) YBaCo₂O_{4.5} and (b,c) LaBaCo₂O_{4.25}.

have rigorously ordered anion vacancies, there is no registry in the phase of anion vacancies between neighboring chain pairs, resulting in the refinement of a disordered structure from diffraction data. The cobalt centers present in the remaining CoO rows within the CoO_{1.75} layers remain five-coordinate. The reduction of YBaCo₂O₅ to YBaCo₂O_{4.5} therefore converts a mixed-valent Co(II/III) phase with cobalt located in five-fold coordinate square-based pyramidal coordination sites into a Co(II) phase in which 50% of the cobalt resides in square-based pyramidal coordination and 50% in highly distorted tetrahedral sites (Figure 11). Bond valence sums calculated for these two coordination sites (5CN = 1.99, 4CN = 1.78) are broadly consistent with Co(II).

Cobalt Coordination Environments in LaBaCo₂O_{4.25}. The anion vacancies within the structure of LaBaCo₂O_{4.25} adopt a more complex arrangement than those in YBaCo₂O_{4.5}, as shown in Figure 10. As a result, the four-fold distorted tetrahedral environments present in LaBaCo₂O_{4.25}, while similar in local geometry to those in YBaCo₂O_{4.5}, are arranged into a different, three-dimensionally ordered network as shown in Figure 10c. In further contrast to YBaCo₂O_{4.5}, LaBaCo₂O_{4.25} has anion vacancies located within the barium–oxygen layers of its structure. This converts one-quarter of the CoO₅ square-based pyramidal sites present in LaBaCo₂O₅ into square-planar CoO₄ centers as shown in Figures 10d and 11c. As a result, LaBaCo₂O_{4.25} contains cobalt in three distinct coordination environments: four-coordinate tetrahedral (50%), five-coordinate square-based pyramidal (25%), and four-coordinate square-planar (25%) (Figures 10 and 11). The anion vacancies within the BaO_{0.75} layers are partially disordered, so the positions of the CoO₅ pyramidal and CoO₄ planar centers are disordered over half the cobalt sites, with the CoO₄ tetrahedra ordered over the other half of the cobalt sites, as shown in Figure 10.

The presence of anion vacancies within the barium–oxygen layers lowers the oxygen stoichiometry to LaBaCo₂O_{4.25}, resulting in an average cobalt oxidation state of +1.75. This is consistent with the location of a Co(I) center at the square-planar coordination site (favored by crystal field stabilization energy) and Co(II) at the pyramidal and tetrahedral sites. Support for this oxidation state assignment comes from the refined

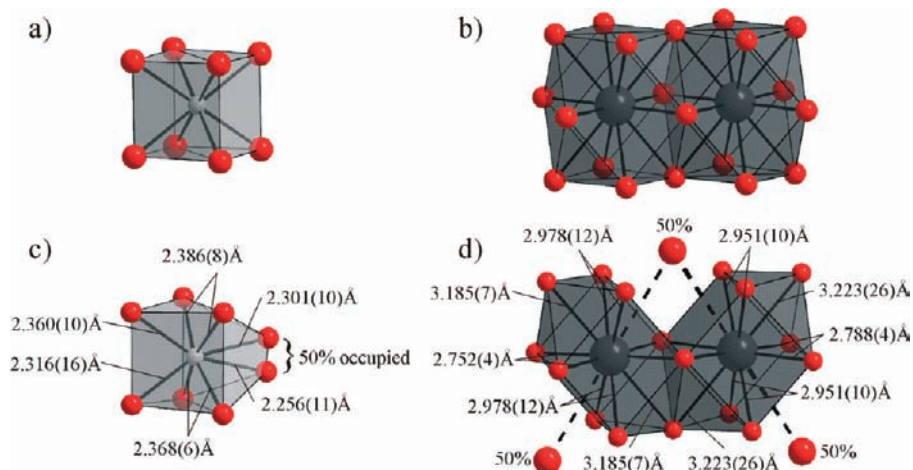


Figure 12. (a) Yttrium and (b) barium coordination polyhedra in YBaCo_2O_5 and the analogous (c) yttrium and (d) barium coordination polyhedra present in $\text{YBaCo}_2\text{O}_{4.5}$.

magnetic structures of the two cobalt phases. $\text{YBaCo}_2\text{O}_{4.5}$ adopts a simple G-type antiferromagnetically ordered phase below 280 K (Figure 6a). $\text{LaBaCo}_2\text{O}_{4.25}$ adopts an identical magnetic ordering scheme below 325 K, except that the ordered moments associated with the CoO_4 planar/ CoO_5 pyramidal sites are almost exactly half those of the CoO_4 tetrahedral sites ($1.61(2) \mu_B$ planar/pyramidal; $3.31(2) \mu_B$ tetrahedral), consistent with a 1:1 disordered arrangement of low-spin, square-planar, $s = 0$, Co(I) centers and high-spin Co(II) centers located on these sites (Figure 6b). Thus, the refined magnetic structure of $\text{LaBaCo}_2\text{O}_{4.25}$ supports the refined crystal structure of $\text{LaBaCo}_2\text{O}_{4.25}$ and the presence of square-planar, low-spin Co(I) centers.

While cobalt(I)-containing oxides are rare, they are not unknown. However, Co(I) centers are usually found in linear coordination in oxides, such as CsK_2CoO_2 or K_3CoO_2 .^{21,22} There are also examples of Co(I)-containing oxides prepared by low-temperature topotactic reductions (e.g., $\text{LaSrCoO}_{3.38}$ and $\text{LaSrCoO}_3\text{H}_{0.7}$ ^{17,20}), but in these cases the coordination environment of the Co(I) centers is ambiguous due to extreme structural disorder. Therefore, to the best of our knowledge, $\text{LaBaCo}_2\text{O}_{4.25}$ is the first unambiguous observation of a low-spin, square-planar Co(I) center in an extended oxide.

Molecular examples of square-planar Co(I) coordination are known, for example in N-heterocyclic dicabene complexes²³ or tetraazamacrocycles²⁴ which are observed to be diamagnetic, consistent with a low-spin electron configuration. However even in molecular species square-planar Co(I) complexes are rare as they are subject to facile ligand additions to form 5-coordinate 18-electron species.

Analysis of the bond lengths of the Co(I) site is complicated by the disordered superposition of this site with a the Co(II) pyramidal site. However, comparison of the Co(I)/Co(II) planar/pyramidal site in $\text{LaBaCo}_2\text{O}_{4.25}$ with the pyramidal $\text{Co}^{\text{II}}\text{O}_5$ site in $\text{YBaCo}_2\text{O}_{4.5}$ reveals that the former site is significantly extended in the equatorial plane with respect to the latter. Bond

valence sums calculated for CoO_5 pyramidal and CoO_4 planar coordination sites extracted from the planar/pyramidal site of $\text{LaBaCo}_2\text{O}_{4.25}$ (Figure 6b) yield values for Co of +1.72, +1.73 and +1.23, +1.23, respectively, consistent with the assigned oxidation states.

Structure-Directing Role of the A-Cations. The different arrangement of anion vacancies in the materials prepared by the topotactic reduction of the two isostructural phases, YBaCo_2O_5 and $\text{LaBaCo}_2\text{O}_5$, is striking. We can rationalize the different behavior of the two A-cation ordered phases by considering the coordination preferences and requirements of the different cations present. Following a logic that has proved successful in the analysis of other topotactically reduced phases,²⁵ it is clear that in order to best satisfy the competing coordination requirements of all the cations in the $\text{REBaCo}_2\text{O}_{5-x}$ phases, oxide ions will be removed from sites which form the strongest bonds to cobalt and the weakest bonds to the A-cations (Ba^{2+} , Y^{3+} , La^{3+}). We can quantify this idea using bond valence sums, as has been demonstrated previously for a number of topotactically reduced phases.²⁵ Considering the structure of YBaCo_2O_5 ,⁶ it can be seen that $\text{BVS}_{\text{Co}} - (\text{BVS}_{\text{Ba}} + \text{BVS}_{\text{Y}})$ gives values of -0.07 and -0.114 for the equatorial and axial anion sites, respectively, consistent with the removal of oxide ions from the equatorial sites of both $\text{REBaCo}_2\text{O}_5$ phases on reduction.

The difference in the ordering of the anion vacancies in the two $\text{REBaCo}_2\text{O}_{5-x}$ phases arises from the differing sizes of Y^{3+} and La^{3+} . It can be seen from the refined structure of $\text{YBaCo}_2\text{O}_{4.5}$ that, on reduction, some of the oxide ions from the $\text{CoO}_{1.75}$ equatorial layers are pushed into the yttrium layer. This has a number of consequences. First, it significantly extends one of the Co–O bonds consistent with a lowering of the average cobalt oxidation state from +2.5 to +2 (Figure 11a). Second, the anion displacement significantly contracts one of the Y–O bonds, so that with a slight displacement of the yttrium a YO_7 coordination site with seven approximately equal bonds can be formed, as shown in Figure 12c. A final consequence of the oxide ion displacement is a lengthening of the corresponding Ba–O distance, such that the coordination number of barium drops from 12 to 10, “losing” one oxide ion due to removal and one due to displacement, as shown in Figure 12d.

(21) Bernhardt, F.; Hoppe, R.; Kremer, R. K. *Z. Anorg. Allg. Chem.* **1994**, *620*, 187–191.

(22) Burow, W.; Brix, J.; Bernhardt, F.; Hoppe, R. *Z. Anorg. Allg. Chem.* **1993**, *619*, 923–933.

(23) Danopoulos, A. A.; Wright, J. A.; Motherwell, W. B.; Ellwood, S. *Organometallics* **2004**, *23*, 4807–4810.

(24) Fujita, E.; Creutz, C.; Sutin, N.; Szalda, D. J. *J. Am. Chem. Soc.* **1991**, *113*, 343–353.

(25) O'Malley, M.; Lockett, M. A.; Hayward, M. A. *J. Solid State Chem.* **2007**, *180*, 2851–2858.

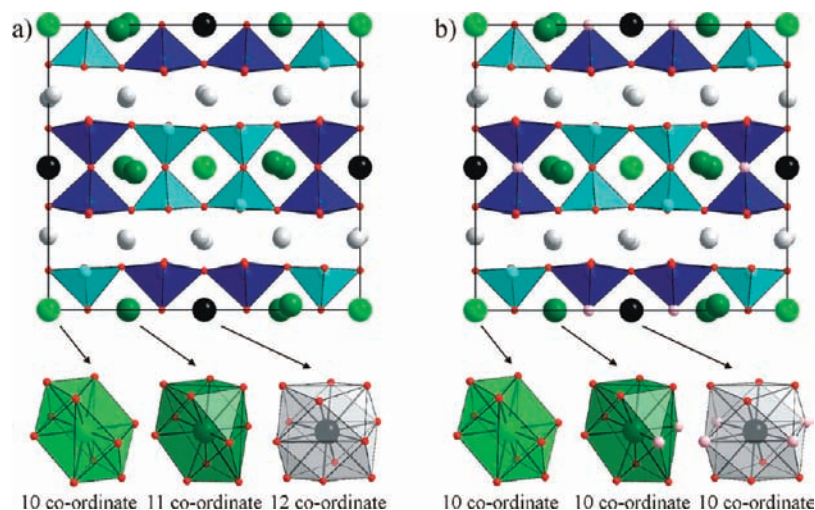


Figure 13. Barium coordination polyhedra in (a) the proposed intermediate phase $\text{LaBaCo}_2\text{O}_{4.5}$ and (b) $\text{LaBaCo}_2\text{O}_{4.25}$. Large pink anion sites are 50% occupied.

Examining the refined structure of $\text{LaBaCo}_2\text{O}_{4.25}$, it can be seen that there is no equivalent displacement of oxide ions from the $\text{CoO}_{1.75}$ layers into the lanthanum layer, as the coordination requirements of the larger La^{3+} ion can be satisfied with an undistorted structure (Figure 10). Examination of the CoO_4 tetrahedra present in $\text{LaBaCo}_2\text{O}_{4.25}$ reveals that the highly extended $\text{Co}-\text{O}$ bond in this phase is directed into the $\text{BaO}_{0.75}$ layer as shown in Figure 11b, further negating the need for a significant anion displacement into the lanthanum layer. The lack of any significant distortion to the $\text{CoO}_{1.75}$ equatorial layers has an important consequence on the barium coordination sites. If we consider the two possible anion vacancy arrangements of the “intermediate” phase $\text{LaBaCo}_2\text{O}_{4.5}$, in which there are anion vacancies in the equatorial layers but not in the barium–oxygen layers (Figure 13), we can see that an ABAB ordering of the CoO and $\text{CoO}_{0.5}$ rows within the equatorial sheets leads to a structure with 11-coordinate barium and 7-coordinate lanthanum. However, if an AABBAABB arrangement is adopted, then 12-, 11-, and 10-coordinate barium sites are formed, lowering the overall lattice energy (Figure 13a). This arrangement also contains CoO_5 coordinations connected through the BaO layer which can be further reduced to form $\text{LaBaCo}_2\text{O}_{4.25}$, in which all the barium sites now have 10-fold coordination (Figure 13b). Conversely, if an AABBAABB arrangement of CoO and $\text{CoO}_{0.5}$ rows within the $\text{CoO}_{1.75}$ layers was adopted in a structure where the equatorial oxide ions are displaced into the RE layers, a highly unfavorable 8-fold coordination for barium is required.

Thus, it can be seen that the differing coordination requirements of the A-cations direct the anion vacancy ordering in these phases. Initially the relative sizes of Ba^{2+} and RE^{3+} favor the

presence of anion vacancies in the CoO_{2-x} equatorial layers. The arrangement of these vacancies and the ultimate sample stoichiometry are further determined by the relative sizes of the RE^{3+} ions. This suggests that if suitable A-site cations are chosen and ordered within perovskite and related structures, they can direct the anion vacancies in topotactically reduced phases to adopt complex, but controllable, ordering patterns, potentially allowing the designed synthesis of novel complex metal–oxygen networks with unusual transition metal cation coordinations.

Acknowledgment. We thank R. Smith for assistance collecting the neutron power diffraction data at the ISIS facility. Experiments at the ISIS pulsed neutron facility were supported by a beam time allocation from the Science and Technology Facilities Council.

Supporting Information Available: Description of the magnetic measurement procedure for samples containing elemental cobalt impurities; thermogravimetric data from $\text{YBaCo}_2\text{O}_{4.5}$ and $\text{LaBaCo}_2\text{O}_{4.25}$; observed, calculated, and difference plots from the structural refinement against neutron powder diffraction data collected from $\text{LaBaCo}_2\text{O}_{4.25}$ at 5 K, 250 K, and room temperature; complete structural and magnetic details of the refinement of $\text{YBaCo}_2\text{O}_{4.5}$ against neutron powder diffraction data at 5, 200, and 250 K; complete structural and magnetic details of the refinement of $\text{LaBaCo}_2\text{O}_{4.25}$ against neutron powder diffraction data at 5 K. This material is available free of charge via the Internet at <http://pubs.acs.org>.

JA910103D